applied sciences

MDPI

Article

Development of Mathematical Model for Coupled Dynamics of Small-Scale Ocean Current Turbine and Generator to Optimize Hydrokinetic Energy Harvesting Applications

Shahab Rouhi [1,2,†], Setare Sadeqi [1,2,†], Nikolaos I. Xiros [1,*,†], Erdem Aktosun [3,†], Lothar Birk [1,†] and Juliette Ioup [2,†]

[1] Bollinger School of Naval Architecture & Marine Engineering, University of New Orleans, 2000 Lakeshore Dr, New Orleans, LA 70148, USA; srouhi@uno.edu (S.R.); ssadeqi@uno.edu (S.S.); lbirk@uno.edu (L.B.)
[2] Department of Physics, University of New Orleans, New Orleans, LA 70148, USA; jioup@uno.edu
[3] Department of Shipbuilding and Ocean Engineering, İzmir Kâtip Çelebi University, Izmir 35620, Türkiye; erdem.aktosun@ikcu.edu.tr
* Correspondence: nxiros@uno.edu
† These authors contributed equally to this work.

Abstract: The primary goal of this study is to develop and test a small-scale horizontal-axis underwater Ocean Current Turbine (OCT) by creating a mathematical model for coupled dynamics aided by a Blade Element Momentum (BEM) simulation-integrated experimental approach. This research is motivated by the urgent need for sustainable energy sources and the vast potential of ocean currents. By integrating mathematical modeling with the experimental testing of scaled model OCTs, this study aims to evaluate performance accurately. The experimental setup involves encapsulating a 3D-printed turbine model within a watertight nacelle which is equipped with sensors for comprehensive data recording during towing tank tests. Through these experiments, we seek to establish correlations between the generated power, force, and rotational speed of the turbine's Permanent Magnet DC (PMDC) motor, which determines the turbine's capability to extract dynamic energy inflow. Moreover, this research aims to provide valuable insights into the accuracy and applicability of theoretical predictions in real-world scenarios by comparing the experimental results with BEM simulations. This combined approach not only advances our understanding of hydrokinetic energy conversion, but also contributes to the development of reliable and efficient renewable energy technologies that address global energy challenges while mitigating environmental impacts.

Keywords: hydrokinetic energy; marine renewable energy; energy conversion; ocean current turbines (OCT); blade element momentum (BEM) theory; towing tank testing; dynamometer testing; small-scale experimental OCT; design evolution; 3D-printed turbine model

check for updates

Citation: Rouhi, S.; Sadeqi, S.; Xiros, N.I.; Aktosun, E.; Birk, L.; Ioup, J. Development of Mathematical Model for Coupled Dynamics of Small-Scale Ocean Current Turbine and Generator to Optimize Hydrokinetic Energy Harvesting Applications. *Appl. Sci.* **2024**, *14*, 7164. https://doi.org/10.3390/app14167164

Academic Editor: Wei Huang

Received: 30 March 2024
Revised: 6 August 2024
Accepted: 7 August 2024
Published: 15 August 2024

Copyright: © 2024 by the authors. Licensee MDPI, Basel, Switzerland. This article is an open access article distributed under the terms and conditions of the Creative Commons Attribution (CC BY) license (https://creativecommons.org/licenses/by/4.0/).

1. Introduction

The urgency for sustainable energy alternatives, fueled by a burgeoning global population, has thrust renewable sources into the forefront of energy discourse [1–3]. Among these alternatives, hydrokinetic energy emerges as a compelling solution [4,5], harnessing the kinetic motion of water bodies like rivers and oceans [6,7]. Its ability to mitigate the deleterious environmental impacts associated with conventional fossil fuels renders it an economically viable and environmentally friendly asset [8–10]. However, despite its substantial potential, the practical implementation of hydrokinetic energy technology remains relatively unexplored, necessitating innovative strategies to facilitate its effective utilization within the energy sector [11,12]. Driven by the finite nature of traditional energy reserves [13,14], the pursuit of alternative sources has catalyzed the development of hydrokinetic turbines [15,16].

Extensive research in hydrokinetic energy conversion has delved into various turbine configurations [17,18], spanning horizontal-axis [19], vertical-axis [20], cross-flow [21],

and oscillating-hydrofoil designs [22]. Notably, studies have revealed the superior performance of hydrokinetic turbines compared to their wind counterparts [23–25], with horizontal-axis turbines emerging as the pre-eminent choice globally [26–28]. In contrast to wind turbines mounted on towers, horizontal-axis hydrokinetic turbines are often secured to the seafloor [29–31], resembling airborne wind turbines in their design and placement [32–34].

Similar to the developmental trajectory of wind turbines, empirical validation through systematic experimentation is paramount for comprehending the behavior of hydrokinetic turbines and optimizing their performance [35,36]. In response to this need, a novel testing approach has emerged, utilizing towing tanks that are commonly employed in maritime engineering for ship design and propulsion research [37]. This approach focuses on the conversion of ocean currents' kinetic energy [38–40], emphasizing the commonality with horizontal-axis turbines used in wind energy [41]. Recognizing the divergence in principles, such as free surface effects and cavitation [42–44], specialized numerical methods have been developed and validated [45,46]. These include simulation tools grounded in Blade Element Momentum (BEM) theory, demonstrating satisfactory representations of experimental turbine performance and offering confidence in their applicability for marine current turbine development [47].

This paper introduces a groundbreaking methodology for the dynamometer testing of hydrokinetic turbines, propelling the field towards standardized empirical assessment [48]. By leveraging towing tanks as a testing platform and integrating sensors to capture vital parameters, this experimental framework not only quantifies energy consumption, but also facilitates the extraction of essential hydrodynamic characteristics, such as torque and power generation, thereby fostering further advancements in the field [49]. Additionally, this paper sheds light on the development of an affordable hydrokinetic turbine tailored for towing tank experimental validation and proof-of-concept demonstrations [50–52]. This accessible turbine model serves as a valuable testbed for evaluating design concepts, optimizing performance, and validating numerical simulations through controlled experiments, ultimately contributing to the maturation and widespread adoption of hydrokinetic energy technologies [53,54].

In this study, we aim to advance hydrokinetic energy conversion technology by focusing on small-scale horizontal-axis underwater OCTs based on rising global energy challenges. We integrate mathematical modeling with experimental testing in our research. Our major goal is to accurately evaluate OCT performance, aided by the development of a mathematical model, by establishing correlations between power generation, force, and turbine motor rotational speed. In this research, we seek to provide insights into the accuracy of theoretical predictions by comparing experimental results with BEM simulations. Also, we introduce a novel dynamometer testing methodology using towing tanks which facilitates the extraction of essential hydrodynamic characteristics. This paper is structured with sections detailing the down-scaling of full-scale OCT, experimental setup, and testing procedures, followed by an analysis of our empirical and mathematical findings. Finally, we highlight our efforts to help improve and make widely available effective hydrokinetic energy technologies.

2. Methodology

2.1. Model Scaling of Full-Scale OCT

The study of hydrofoil designs is very important in hydrodynamics engineering. Hydrofoils play a critical role in determining the lift and drag characteristics of the propeller and turbine [55]. In this investigation, we focus on 25 specific hydrofoil coordinate files labeled using a systematic naming convention as shown in Table 1. Additionally, we consider the rotor diameter and rotational speed, essential parameters influencing rotorcraft performance [56]. The hydrofoil coordinate files were obtained, each containing the respective data points that define the shape of the hydrofoil. These foils were analyzed using computational tools for processing hydrofoil data. The hydrofoil shapes were then

visualized and compared to identify variations in thickness and geometry along the radial elements. The full-scale propeller that SNMREC tested and used at Florida Atlantic University is a remarkable engineering feat [57]. It possesses a number of noteworthy qualities that enhance its effectiveness and performance [58]. A hydrofoil of type FX-77-W [59,60], a particular hydrofoil form renowned for its advantageous properties, was used to create the propeller [61]. The family of hydrofoils to which it belongs actually uses a naming scheme where the last three digits roughly equate to the thickness ratio multiplied by 1000.

Table 1. The hydrofoil types that are used for the propeller design for the scaled model and their properties, as seen in [57,59–61].

Hydrofoil#	Hydrofoil Label	Percentage Thickness
1	FX77-02349-01	23.49%
2	FX77-02349-02	23.36%
3	FX77-02349-03	23.01%
4	FX77-02349-04	22.73%
5	FX77-02349-05	22.23%
6	FX77-02349-06	21.62%
7	FX77-02349-07	20.92%
8	FX77-02349-08	20.12%
9	FX77-02349-09	19.25%
10	FX77-02349-10	18.32%
11	FX77-02349-11	17.34%
12	FX77-02349-12	16.33%
13	FX77-02349-13	15.30%
14	FX77-02349-14	14.86%
15	FX77-02349-15	14.42%
16	FX77-02349-16	14.00%
17	FX77-02349-17	13.60%
18	FX77-02349-18	13.23%
19	FX77-02349-19	12.89%
20	FX77-02349-20	12.58%
21	FX77-02349-21	12.25%
22	FX77-02349-22	11.94%
23	FX77-02349-23	11.64%
24	FX77-02349-24	11.34%
25	FX77-02349-25	11.07%

The objective of the scaling was to investigate the hydrodynamic performance of a propeller at reduced dimensions while maintaining similarity with the full-scale model. In the study of propellers and hydrodynamics, the advance ratio (J) and Froude number (Fr) are important dimensionless factors. The propeller's effectiveness and performance are determined by the advance ratio, and reliable scaling for experimental studies is made possible by Froude similarity. One of the main advantages of using towing tanks is the ability to control the experimental conditions, such as towing speed, propeller rotational speed, and environmental parameters. These controlled experiments provide valuable data for validating computational fluid dynamics (CFD) simulations and improving our understanding of propeller hydrodynamics. The restrictions applied on the advance ratio (J), towing speed U, and Reynolds number (Re) are crucial in defining the operating conditions and hydrodynamic performance of the propeller in this study. Operating within these specific ranges ensures that the experimental results are representative of real-world conditions and allows for a more accurate and insightful analysis of the propeller's behavior under different flow regimes and operating conditions.

In this particular research, the advance ratio was restricted to be within the range of $0.032 < J < 0.79$. The propeller was used at relatively low forward velocities in relation to its rotational speed and diameter, as indicated by the lowest limit of 0.032 ($J > 0.032$). In this case, the propeller runs inefficiently and generates less thrust for a given rotational

speed. The upper limit of the advance ratio, 0.79 ($J < 0.79$), indicates that the propeller operates more efficiently, with a more significant proportion of the forward velocity due to the rotational speed. When the propeller operates in this range of the advance ratio, it can produce higher thrust and provide better propulsion performance. Based on the small-scale analysis, the most suitable current velocity for the carriage was found to be restricted within the range of 0.1 m/s < U < 2.450 m/s. At the lower limit of carriage speed 0.1 m/s ($U > 0.1$ m/s), the propeller operates in a generally calm water flow with low current velocities. In this scenario, the propeller may experience decreased overall performance because of the limited quantity of kinetic energy in the fluid. The upper limit of 2.450 m/s ($U < 2.450$ m/s) indicates that the propeller operates in faster-flowing water conditions. In this regime, the propeller experiences higher flow velocities, potentially leading to increased thrust and better performance. According to the scale-down procedure, the Reynolds number (Re) is given as $2 \times 10^5 < Re < 7 \times 10^6$ in this study.

BEM theory is a well-known technique used to analyze the performance of turbines. In this study, a unique BEM algorithm developed in the MATLAB (2023b) environment was used to consider the specific flow conditions and rotor characteristics. This unique BEM algorithm had a good capacity to make an estimation of various parameters, such as differential torques, thrusts, and power, for the turbines under investigation. To validate the predictions obtained from the BEM algorithm and conduct proof-of-concept testing, a small-scale three-bladed horizontal underwater turbine was constructed. Utilizing a small-scale turbine is a cost-effective approach compared to full-scale testing. This small-scale turbine served as a prototype for testing and numerical model verification. For the experimental setup, an electrical system was required to meet the necessary requirements and measure the generated power. OCT generates power based on local forces, primarily the lift force acting on the rotor blades. In addition, to prevent any structural damage to a full-scale prototype, the undesirable forces acting on the carriage were estimated and analyzed. To estimate the nominal generated power at different carriage speeds and rotor blade rotational speeds, the following method was employed. The carriage speed was used to mimic the motion of the water current, which contains kinetic energy. The tip speed ratio was adjusted to achieve optimal power production at a constant carriage speed. This adjustment was accomplished by varying the rotational speed of the rotor blades.

Prior to the design process, several considerations were made. It was crucial to define the expectation for the entire system and determine the best approach for assembling the system with the required components. Due to the limited carriage speed at the UNO towing tank, the DC machine must reach steady-state rotational speeds before functioning as a generator. Therefore, electricity was supplied to the motor using a power supply to achieve the desired speed. Additionally, each circuit element within the system had to be carefully selected and sized to ensure appropriate operation. By incorporating these considerations and implementing the described methodology, this study aims to develop an appropriate design and gather the necessary data for further analysis and evaluation of the OCT's performance.

2.2. Design and Construction of Small-Scale OCT

Designing a small-scale propeller in SolidWorks (2024) involves a systematic process:

- Importing the coordinates of 25 distinct hydrofoils into SolidWorks, which define their shapes;
- Defining the blade planes;
- Sketching each blade within its respective plane;
- Repeating the sketching process for all 25 hydrofoils;
- Applying the chord length, twist, and sweep angles to each hydrofoil;
- Creating the 3D model;
- Adding the hub and shaft.

In our propeller design, we twisted each blade along its length to enhance performance by evenly distributing lift and increasing efficiency. This customized twist and sweep for each blade section created the desired propeller shape.

A 3D model of the propeller was built as seen in Figure 1a, after sketching and adjusting the blade sections for twist and sweep, as seen comprehensively in Figure 1b. Various tools were employed to loft or sweep the sketched sections, ensuring a seamless transition and continuous blade shape. Additionally, the central hub and shaft were separately sketched and integrated with the blades to form the final propeller, following scale-down calculations and dimensions.

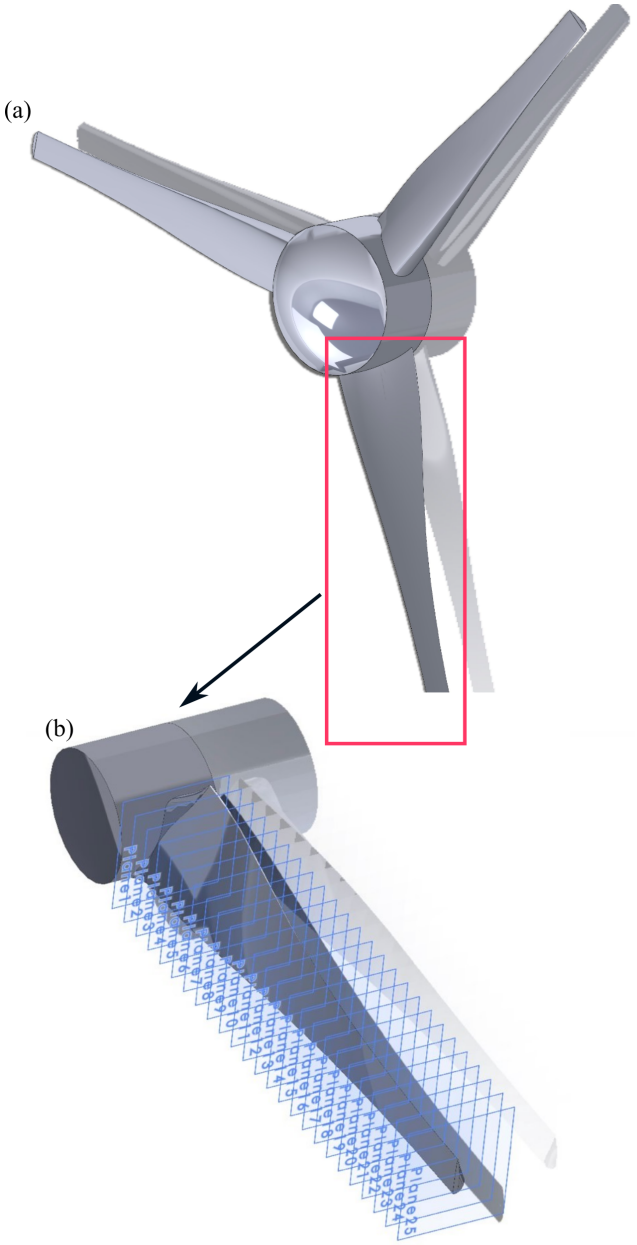


Figure 1. (**a**) Design of three-bladed rotor. (**b**) Hydrofoil sketch using Solidworks.

To manufacture the small-scale propeller, we utilized a 3D printer at the University of New Orleans and opted for carbon fiber filament due to its specific advantages. Carbon fiber offers exceptional stiffness, strength, and fatigue resistance, aligning well with the requirements of our experiment. Its outstanding strength-to-weight ratio significantly reduces the overall weight of the propulsion system, thereby enhancing performance

and efficiency. Compared to traditional materials like metal, carbon fiber is much lighter while maintaining impressive structural integrity. This enables the construction of thin, lightweight blades capable of withstanding the hydrodynamic forces experienced during the experiment. The high tensile strength of carbon fiber contributes to the durability of the propeller, reducing wear and tear and resulting in cost savings and improved reliability. Additionally, carbon fiber's resistance to corrosion and superior fatigue resistance ensure a longer operational life, crucial for withstanding the harsh conditions of the towing tank environment and dynamic loads experienced during the experiment. Overall, carbon fiber filament offers a combination of light weight, strength, and durability that makes it an ideal choice for propeller construction, leading to improved performance and longevity.

The hydrokinetic turbine nacelle was designed following the ITTC guidelines and created using SolidWorks, a piece of CAD software known for precise modeling. To ensure the safety of the electronic components and sensors during testing, the nacelle was divided into two parts. This separation protected delicate parts from potential damage or interference during testing.

The first segment of the model or "insert" serves as a protective enclosure for the instruments. It consists of two parts: a base piece and a cap. The base piece provides a stable platform for the motor and sensors, ensuring their secure positioning during testing. Figure 2a provides a visual representation of the base piece of the insert and its function.

The cap is the upper piece of the insert shown in Figure 2b. The main purpose of the cap of the insert is to shield and safeguard the instruments housed within from external factors that could impact their performance. This includes protecting the components from potential leaks from the submerged nacelle in the towing tank, which could compromise the accuracy and safety of the experimental setup.

The insert, consisting of a base piece and cap, provides a robust and protective environment for the PMDC motor and sensors during hydrokinetic turbine testing. This setup ensures reliability and security, enhancing the precision and accuracy of collected data. Designed to fit securely into a watertight torpedo nacelle, the insert serves a specific purpose in the testing process. The torpedo nacelle, illustrated in Figure 2c, acts as a second layer of security, designed to be fully submerged during testing, ensuring the components inside stay dry and protected from water ingress, thereby maintaining their safety and security.

The separation of the model into two segments—the insert and the torpedo nacelle—offers several advantages. Firstly, it simplifies the assembly and disassembly process of the turbine model, ensuring a straightforward and secure connection between the insert and the nacelle. Secondly, this division provides an extra layer of protection for the sensitive electronic components and sensors within the turbine model in the underwater environment. By placing the insert inside the watertight nacelle, critical parts are isolated from the surrounding water, eliminating the risk of damage due to water exposure.

The nacelle, manufactured using a Prusa i3 MK3S+ 3D printer, as seen in Figure 2d, employed a water-resistant PETG filament for durability in the testing environments. PETG's strength and resilience make it suitable for harsh conditions, such as submerged testing. Additional steps were taken to reinforce the model and ensure watertightness. An epoxy coating was applied to seal any gaps or openings, preventing water damage to the internal components. The PETG filament offers unique advantages, including excellent layer adhesion, warp resistance, reduced shrinkage, higher density, and chemical resistance to acidic and alkaline compounds. It also provides flexibility and resistance to chemicals and moisture, allowing for printing on various surfaces, such as glass, acrylic, and tape, while remaining odorless during printing. These characteristics, combined with protective coatings, contribute to the creation of a durable and reliable turbine model capable of withstanding the rigors of submerged testing.

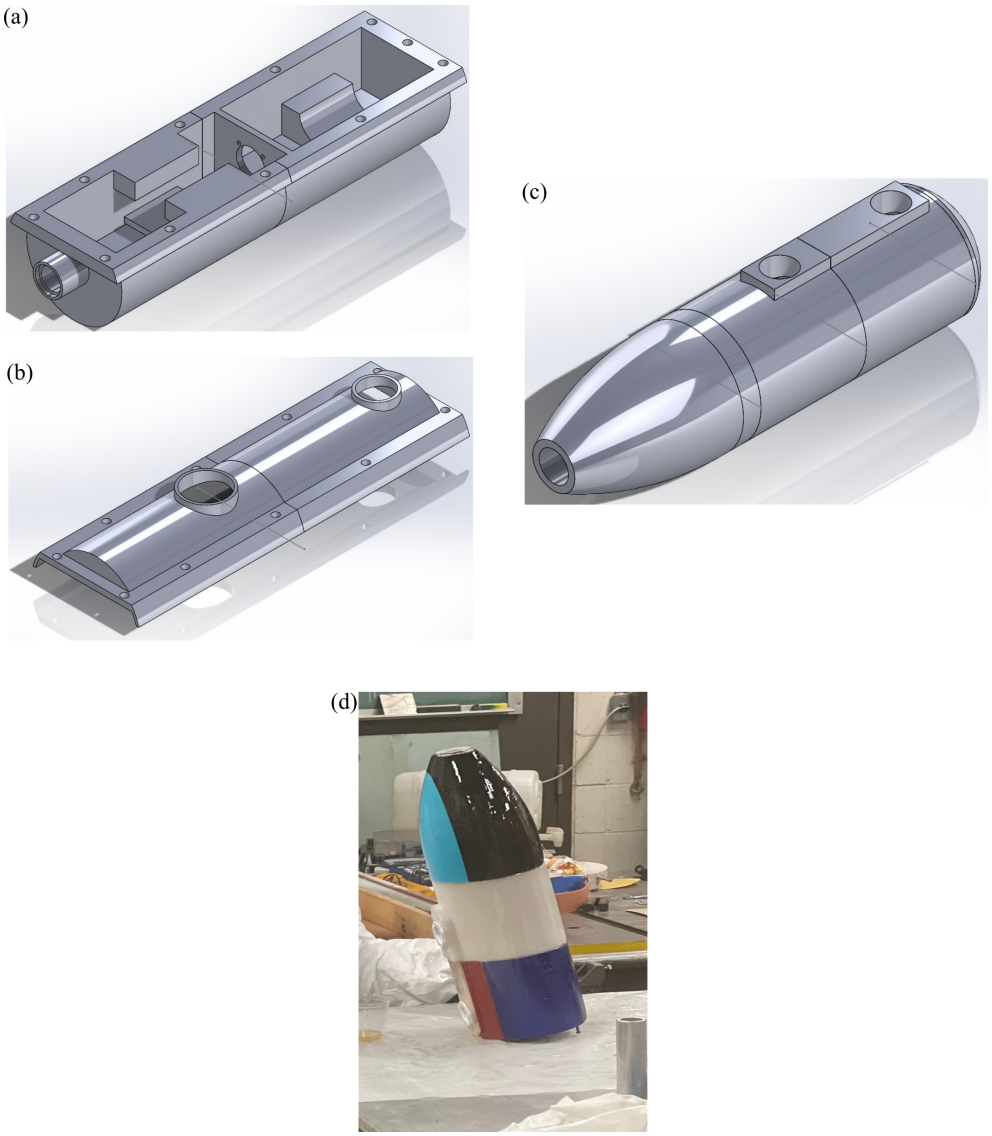


Figure 2. (**a**) SolidWorks sketch of the insert base, (**b**) SolidWorks sketch of the insert cap, (**c**) SolidWorks sketch of the nacelle, (**d**) and nacelle coated with epoxy. Parts (**a**,**b**) represent separate components of the insert. These components slide into the nacelle. The nacelle itself is a distinct entity from the insert components.

2.3. Experimental Details

The towing tank is a specialized laboratory facility utilized for conducting hydrodynamic tests on various models, including ships, offshore structures, and hydrokinetic turbines. The towing tank at the University of New Orleans is a rectangular basin with specific dimensions: 30.8 m long, 4.6 m wide, and 2.4 m deep.

The tank is equipped with a carriage system that runs along rails installed along the length of the tank. This carriage system is driven by a cable and a 10 HP AC motor, capable of a maximum speed of 3.66 m per second. The speed of the carriage can be digitally controlled utilizing an electric-powered horizontal planar motion system (PMM). The main purpose of the carriage system is to support and tow the hydrokinetic turbine model during the testing process. The model is mounted on a structure that can be adjusted in terms of depth, angle, and orientation comparatively with the water stream. This customizability allows for the study of the turbine's performance under different working conditions. This model is associated with a carriage system utilizing cables and pulleys, enabling it to be towed at various speeds and angles to simulate different water stream conditions. To maintain consistent testing conditions, the towing tank is equipped with filtration and

treatment systems. Consequently, water circulates within the tank, and any pollutants are eliminated. Moreover, the water temperature and salt concentration are observed and controlled to maintain exact and reliable testing conditions.

The hydrokinetic turbine model features an electric motor which can be run as a generator, and various sensors. They are all housed inside the insert. Specifically, a PMDC motor of the type DCX 35 L (Maxon Precision Motors, Inc., Taunton, MA, USA), with a power rating of 80 to 120 Watts, was used as the motor/generator. To control its operation, the PMDC motor was associated with a driver, which allowed exact control of the motor's speed. To adjust the motor speed, a variable DC voltage source was connected to the driver. By varying the input voltage to the motor, its rotational speed could be adjusted as desired for testing purposes. The PMDC motor utilized in the hydrokinetic turbine model has a speed rating of 8130 RPM (Revolutions per Minute). However, to suit the scaled-down size of the turbine model, a planetary gear-head of the sort GPX 37 (Maxon Precision Motors, Inc., Taunton, MA, USA), with a reduction ratio of 16:1 was utilized to reduce the speed output of the motor. The decision to employ a gear-head with a reduction ratio was necessary and essential due to the fact that the hydrokinetic turbine model is restricted to a more limited rotational speed.

In the experimental setup for the hydrokinetic turbine model, different sensors and equipment were installed to measure and control various aspects of the system. The detailed specifications can be found in the product datasheets.

- TRS605 Rotational Force Sensor (FUTEK Advanced Sensor Technology, Inc., Irvine, CA, USA): This non-contact shaft-to-shaft rotary torque sensor, equipped with an encoder, was placed between the motor and propeller shafts. The reason was to precisely evaluate the driving torque applied to the system and to quantify the rotational speed of the turbine. The accuracy of the TRS605 Rotational Force Sensor was within ±0.1%.
- ESCON 50/5 servo controller (Maxon Precision Motors, Inc., Taunton, MA, USA): This motor driver, known as an ESCON 50/5 servo controller, was used to maintain a setpoint motor rotational speed and adjust it to maintain a desired speed during testing. The accuracy of the ESCON 50/5 servo controller was within ±0.05%.
- Current and voltage sensors: to measure the electrical power created by the hydrokinetic turbine, current sensors (ACS712, SparkFun Electronics, Boulder, CO, USA) and voltage sensors (DC0-25V, MAKERS Electronics, Alexandria, Egypt) were installed. These sensors allowed us to screen the electrical current moving through the system and the voltage across the PMDC motor, which are fundamental for computing the generated power. The accuracy of the ACS712 current sensor was within ±1.5% and the accuracy of the DC0-25V Voltage Sensor was within ±0.5%.
- Temperature and humidity sensors: For safety and performance monitoring, temperature and humidity sensors were installed. Two sensors of type SHT30 (Sensirion, Stäfa, Switzerland) and two of type DHT22 (Kuongshun Electronic, Shenzhen, China) were utilized to measure the temperature and humidity levels inside the turbine nacelle. The accuracy of the SHT30 temperature and humidity sensor was within ±2% for humidity and ±0.3 °C for temperature, and the accuracy of the DHT22 temperature and humidity sensor was within ±2% for humidity and ±0.5 °C for temperature.

Table 2 provides a clear overview of the sensors used, their accuracy, and their respective purposes in the experimental setup.

The insert setup, which includes all these sensors and equipment, is shown in Figure 3.

To process and analyze these data, a data acquisition system was employed. In this case, a National Instruments (NI) SCXI-1000 data acquisition system (Austin, TX, USA), integrated with LabVIEW software (v.8.5.1), was used. This system is capable of gathering analog signals from various sensors. The data collected by these sensors are indispensable for understanding the presentation and conduct of the hydrokinetic turbine model during testing. By estimating force, rotational speed, electrical current, voltage, temperature, and humidity, we can obtain comprehensive information on the turbine's proficiency, power generation capabilities, and safety boundaries.

Table 2. Summary of sensors used in the experimental setup, including accuracy and purpose.

Sensor	Accuracy	Purpose
TRS605	±0.1%	Evaluate driving torque and quantify turbine speed
ESCON50/5	±0.05%	Maintain setpoint motor speed during testing
ACS712	±1.5%	Measure electrical current through the system
DC0-25V	±0.5%	Measure voltage across the PMDC motor
SHT30	±2% (humidity), ±0.3 °C (temperature)	Monitor temperature and humidity inside the turbine nacelle
DHT22	±2% (humidity), ±0.5 °C (temperature)	Monitor temperature and humidity inside the turbine nacelle

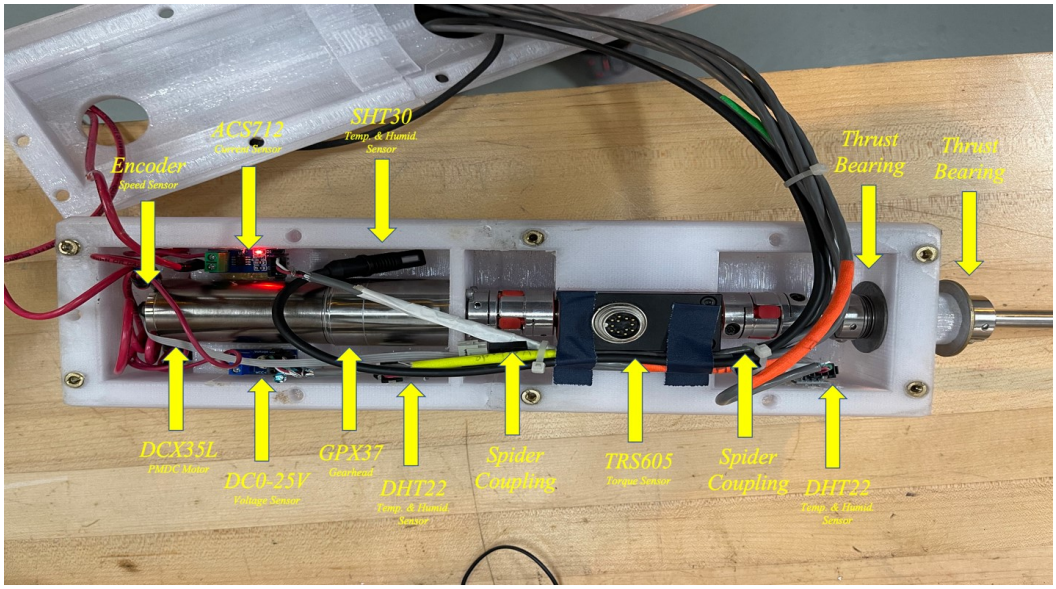


Figure 3. The electric instrument setup for the hydrokinetic turbine model contains various sensors and equipment to measure and control system parameters, including a TRS605 Rotational Force Sensor, an ESCON 50/5 servo controller, current and voltage sensors, and temperature/humidity sensors for comprehensive monitoring.

The testing procedure for understanding the hydrodynamic characteristics of the hydrokinetic turbine consists of several meticulously planned steps, ensuring accurate and reliable data collection.

- Positioning the Hydrokinetic Turbine Model
  Before conducting the experiments, the hydrokinetic turbine model is carefully positioned in the towing tank. This initial step is critical as it sets the foundation for all subsequent measurements and observations. The turbine model is situated appropriately relative to the towing arm, ensuring that it remains stable and aligned throughout the testing process. The insert part containing the electro-machine and sensors is securely connected to the torpedo nacelle, ensuring a watertight seal. This assembly is crucial for preventing water ingress, which could potentially damage sensitive electronic components and compromise data integrity. The precision in positioning the turbine model guarantees that the experimental setup accurately reflects real-world conditions, thereby enhancing the validity of the results.
- Submerging and Towing the Turbine Model
  Once the turbine model is securely placed in the towing tank, it is submerged and prepared for the towing process. The model is towed through the water at a preselected speed, which can be adjusted based on the specific requirements of the test. This controlled towing process simulates various flow conditions that the turbine would encounter in an actual operational environment. During this phase, sensors

installed on the model play a crucial role. These sensors, strategically placed within the turbine structure, continuously record data on key parameters such as torque, speed, and other relevant metrics. This real-time data acquisition enables a detailed analysis of the turbine's performance under different hydrodynamic conditions.

- Data Collection and Analysis
  After the towing process is complete, the data collected from the sensors undergo thorough interpretation. This step involves analyzing the recorded parameters to assess the turbine's hydrodynamic performance. The data are scrutinized to identify patterns and correlations that provide insights into the efficiency and effectiveness of the turbine design. Parameters such as torque and power are critical indicators of the turbine's ability to convert kinetic energy from water flow into mechanical energy. By examining these metrics, we can evaluate the turbine's performance and identify areas for improvement.
  Depending on the results obtained from the experimental tests and data analysis, further testing may be necessary to refine and improve the turbine's design. If certain aspects of the turbine's performance need enhancement or if specific conditions require additional evaluation, iterative testing allows us to make necessary adjustments to the turbine model and reiterate the testing process. This iterative approach ensures continuous improvement and optimization of the turbine design.
- Implications and Future Directions
  The comprehensive data collected during these experiments not only validate the current turbine design but also offer valuable insights for future improvements. By understanding the hydrodynamic characteristics of the turbine under various flow conditions, we can optimize the design for enhanced performance and efficiency. The iterative process of testing, data analysis, and design refinement is fundamental to advancing hydrokinetic turbine technology.

Moreover, this experimental procedure establishes a standardized method for evaluating hydrokinetic turbines, contributing to the broader field of maritime engineering. Future work could involve testing different turbine configurations, materials, and sensor technologies to further enhance our understanding and the performance of hydrokinetic energy systems.

Figure 4 provides a visual representation of the prototype turbine submerged in the towing tank, illustrating the experimental setup. The towing tank environment is carefully controlled to minimize external influences that could affect the results. This controlled environment ensures that the observed performance characteristics are solely attributable to the turbine design and the towing conditions.

The detailed and methodical experimental procedure outlined here ensures the collection of high-quality data, providing a robust foundation for evaluating and improving hydrokinetic turbine designs.

To evaluate the hydrodynamic characteristics of the turbine, various fluid-related parameters are assessed, which are available in Table 3.

Table 3. Fluid flow parameters under towing tank test conditions.

Experimental Parameters	Units	Values
Towing Speed	m/s	0.05–1.95
Kinematic viscosity	m^2/s	1.0334×10^{-6}
Dynamic viscosity	Pa/s	1.0318×10^{-3}
Density	kg/m^3	998.4

In addition, the specifications of the propeller are given in Table 4.

Table 4. Blade properties of the scaled model under towing tank test conditions.

Blade Properties	
Rotor diameter	0.25 m
Number of blades	3
Airfoil	FX-77-W
Material	Stratasys ABS-Based Carbon Fiber Filament

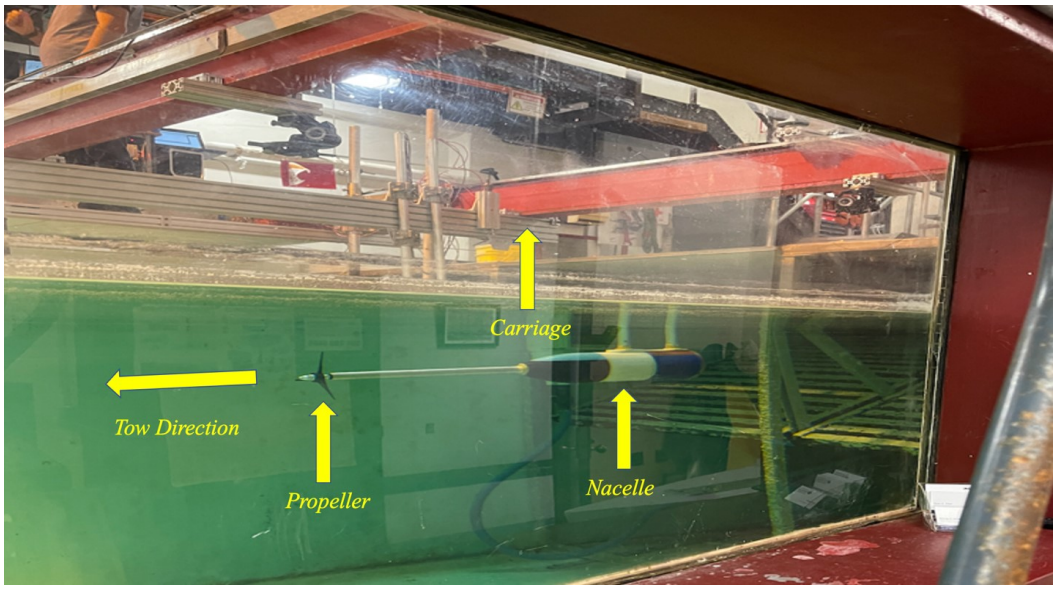


Figure 4. Hydrokinetic scaled model turbine testing with essential operational components for performance evaluation.

Overall, this testing methodology was designed to gain a comprehensive understanding of the hydrokinetic turbine's hydrodynamic characteristics.

3. Results and Discussion

The scaled model of the turbine is towed in the fluid at a specific range of flow speeds. Various sensors are utilized to gather comprehensive data during the towing process. These sensors include current and voltage sensors, which measure the electrical power generated by the scaled model of the turbine, a torque sensor to capture the rotational force applied to the scaled model, and temperature and humidity sensors for security purposes within the system.

However, one might observe that a restriction exists in the testing facility which primarily comes from the length limitation of the towing tank. This may result in the turbine not having sufficient time to reach the chosen steady-state speed condition during the towing process, mainly due to this restriction. We apply a specific approach in order to overcome this towing tank restriction and ensure that our scaled model operates at the determinated speed during the towing tests. The PMDC motor serving as the prime actuator is initially powered to reach the steady-state speed before the carriage initiates towing of the turbine model. After reaching the steady-state speed, the carriage initiates towing the turbine model at the designated speed. The power consumption of the PMDC motor fluctuates in response to the dynamic force exerted by towing the turbine through the fluid throughout the towing process. The variation in power consumption observed by the PMDC motor from its initial steady-state operation to the towing stage characterizes the distinct energy exerted by inflow [62]. The dynamic energy is captured by the hydrokinetic turbine propeller and transformed into rotational kinetic energy [63]. Figure 5 presents the rotational speed of the PMDC motor, measured consistently at 500 rpm, while the system is towed at a speed of 6 feet per second. The plotted data, shown over time, reveal

remarkably stable performance of the motor throughout the towing operation. The black line in the graph, which represents the rotational speed, remains mostly flat, indicating minimal fluctuation around the 500 rpm mark.

A closer inspection of the data shows that the rotational speed exhibits a deviation of 5 rpm, underscoring the motor's consistency and reliability. This stability is crucial for applications requiring the precise control of rotational speed under varying load conditions. This consistent performance can be attributed to the motor's design and the control system's effectiveness in maintaining a steady rotational speed despite potential external disturbances. This characteristic is particularly important for our application, where maintaining a constant speed is essential for operational efficiency determination.

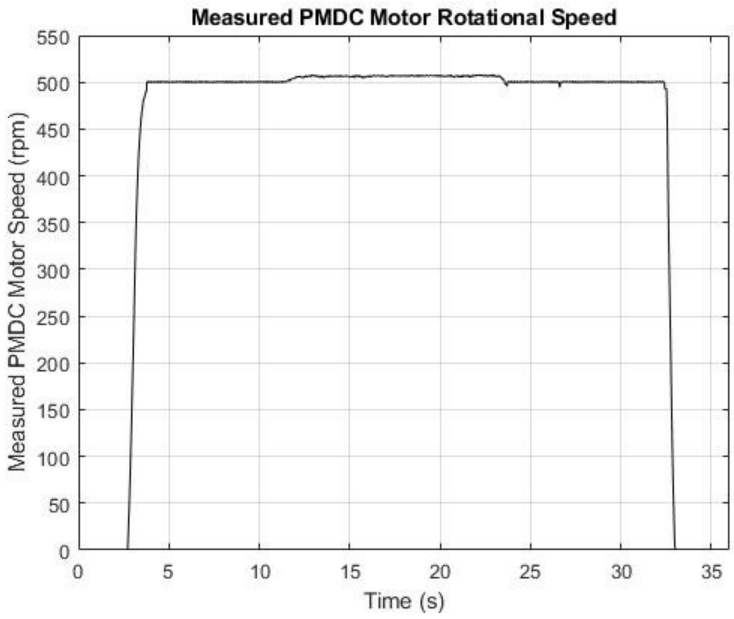


Figure 5. The experimental rotational speed profile of the PMDC motor throughout the towing operation.

Figure 6 displays a graph depicting the electrical current waveform recorded at a towing velocity of 6 ft/s over time. As the hydrokinetic turbine model is propelled through the fluid flow at this velocity, the motor current waveform reveals explicit characteristics throughout the towing process.

A prominent feature of the waveform is the observed decrease in motor current values during the towing process. This decline can be attributed to the dynamic energy supplied by the water flow. As the water streams across the turbine propeller blades, it transfers energy to the turbine, inducing rotation and facilitating power generation. The hydrokinetic turbine effectively harvests this dynamic energy, converting it into rotational motor energy.

Analyzing the data, we observe a significant reduction in motor current from an initial peak value of 2.71 amps to a steady-state value of 1.39 amps. This trend indicates that as the turbine continues to rotate, the current drawn by the motor decreases proportionately. Despite the constant rotational speed of the motor, the decrease in motor current suggests enhanced power extraction by the turbine propeller blades from the water flow. This inverse relationship between motor current and power generation efficiency highlights the turbine's ability to harness kinetic energy from the water effectively. The fluctuations in the motor current waveform directly reflect the performance and power generation capacity of the scaled turbine model.

These results imply that as the turbine blades become more effective in capturing and converting the kinetic energy of the flowing water, less electrical current is required to maintain the motor's rotational speed. This efficiency can be crucial for optimizing the design and operation of hydrokinetic turbines, particularly in applications where maximizing power extraction is essential.

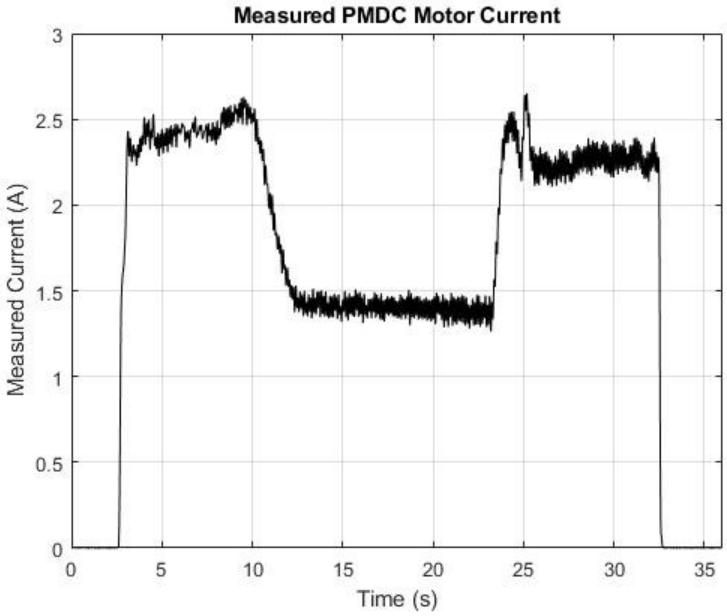


Figure 6. The experimental measurements of the motor current during the towing tank testing.

Future research could focus on exploring the effects of varying towing velocities and blade designs on the motor current waveform. Additionally, employing advanced computational models to study the flow dynamics around the turbine blades could provide deeper insights into the mechanisms of energy transfer and conversion, ultimately guiding the development of more efficient hydrokinetic turbine systems.

Figure 7 shows a graphical representation of the generated power across different carriage speeds during the experimental testing of the scaled hydrokinetic turbine. The measurements were conducted by towing the turbine model at varying carriage speeds, ranging from 0 to 6.5 ft/s (0 to 1.98 m/s). The rotor propeller operated at a consistent rotational speed of 500 rpm, with the input voltage maintained at approximately 12 V. Notably, the voltage amplitude showed minimal fluctuations throughout the towing test.

The graph depicts the fluctuations in the generated power output of the hydrokinetic turbine across the different carriage speeds. The maximum recorded generated power reached 16.7 W, with this peak output observed when the turbine was towed at a velocity of 1.98 m/s. However, despite achieving a peak power output of 16.7 W, the overall performance of the turbine did not meet the optimal expectations.

This suboptimal performance can be attributed to the implementation of a planetary gear-head to achieve a slow driving mechanism within the scaled turbine. While the gear-head effectively reduced the turbine's rotational speed as intended, it was not originally designed for use as a generator and therefore presented some drawbacks. The gear-head introduced inefficiencies, leading to reduced efficiency in power generation.

Despite this suboptimal performance, the experiment exhibited stable body disposition and consistent power generation. The consistent power output, despite the gear-head inefficiencies, suggests that the turbine model maintains stable operation under varying towing speeds. This stability is critical for practical applications, where fluctuating water flow conditions can impact performance.

Figure 8 illustrates how the average generated power changes as the carriage speed increases from 0 to 2 m/s when comparing both the experimental and Blade Element Momentum (BEM) simulation results. The generated power serves as an indicator of the system's power output, where an underwater current turbine converts fluid flow kinetic energy into electrical energy.

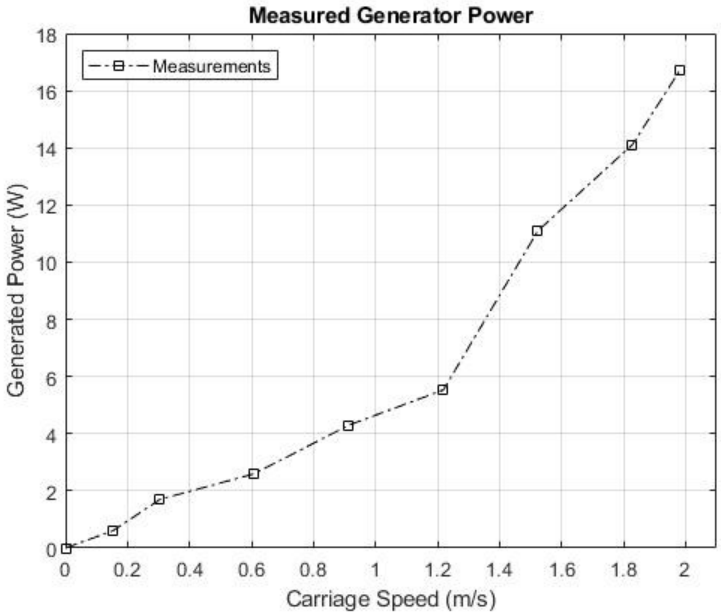


Figure 7. Generated power across different carriage speeds during experimental testing of scaled hydrokinetic turbine.

Both the experimental findings and the BEM simulation results indicate a consistent trend: as the carriage speed increases, the generated power also increases. This observation aligns with theoretical expectations, as increased fluid speed translates to greater energy available for the turbine blades to harness.

A detailed analysis of the plot reveals that for carriage speeds up to 1.2 m/s, the generated power from the BEM simulations is slightly higher than the experimental results. The experimental data show a mean power output of 5.8 W at 1.2 m/s. In contrast, the BEM simulations show a mean power output of 7.9 W for the same speed, indicating systematic overestimation by the simulations.

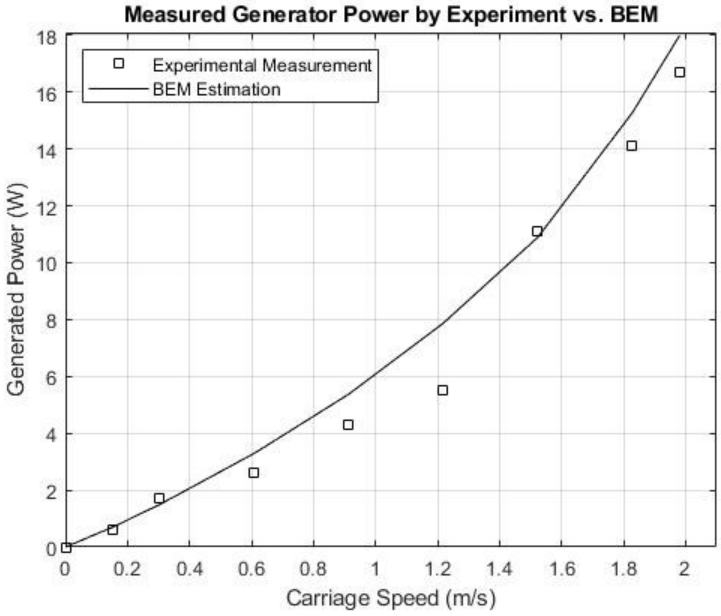


Figure 8. Comparison of average generated power values with increasing carriage speed from 0 to 2 m/s from experimental and BEM simulation results.

However, as the carriage speed approaches 2 m/s, the generated power estimated by the BEM calculations and the experimental results become closer. Specifically, at 2 m/s, the BEM simulations indicate a peak power output of 18.1 W, while the experimental results show a peak power output of 16.3 W. The discrepancy between the experimental data and the BEM simulations at lower speeds suggests that the performance of the scaled OCT model might have been somewhat overestimated by the simulations for lower speeds.

These differences between the experimental data and the BEM simulations could be attributed to several factors. One possibility is measurement error due to the experimental setup or the equipment used to measure the generated power, which might not have been accurate enough. Additionally, some of the intricate hydrodynamic effects that manifest in an actual OCT, particularly at various water speeds, may not have been fully captured or accurately represented by the BEM simulations. This includes complex turbulence effects and three-dimensional flow phenomena that are challenging to model accurately with the BEM method.

Figure 9 illustrates a graph depicting the measured generated torque as a function of carriage speed during the experimental testing. The graph demonstrates direct proportionality between the generated torque and the output power of the turbine. This means that as the power output of the turbine increases, the torque produced by the turbine also increases.

A detailed analysis of the data reveals that the generated torque increases from 0 to 0.29 N·m as the carriage speed increases from 0 to 2 m/s. This trend underscores the direct relationship between the kinetic energy of the fluid flow and the mechanical output of the turbine. The statistical analysis shows a strong correlation between carriage speed and generated torque.

Moreover, the analysis indicates that the turbine operates within safe torque limits across the tested speed range, mitigating the risk of mechanical damage. However, it is crucial to ensure that the torque remains within optimal levels to avoid inefficiencies and potential damage to the generator.

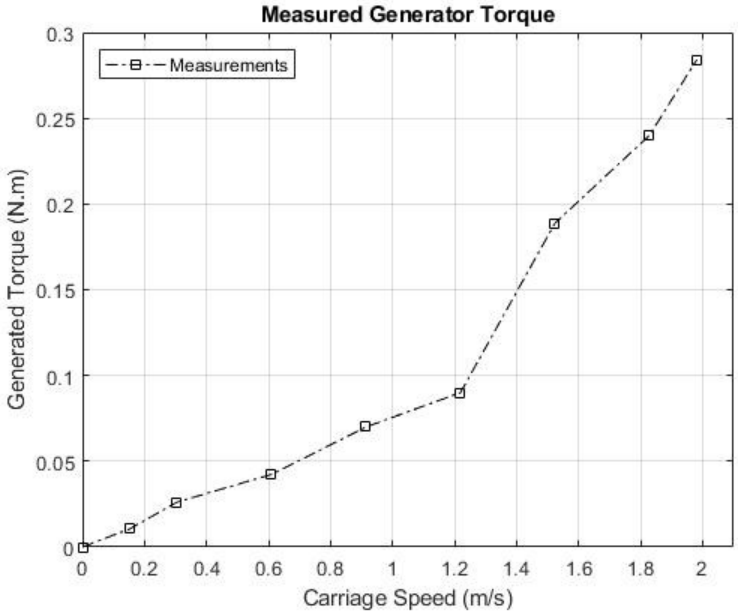


Figure 9. Generated torque across different carriage speeds during experimental testing of scaled hydrokinetic turbine.

Figure 10 illustrates the relationship between carriage speed and generated torque for both the experimental and BEM simulation results. The twisting force exerted by the underwater current turbine blades, referred to as generated torque, facilitates the rotation of the turbine's rotor to generate electricity. The upward sloping trend in the graph indicates

that as the carriage speed is increased from 0 to 2 m/s, the generated torque also increases, ranging from 0 to 0.3 N·m in the BEM simulation and from 0 to 0.28 N·m in the experiment.

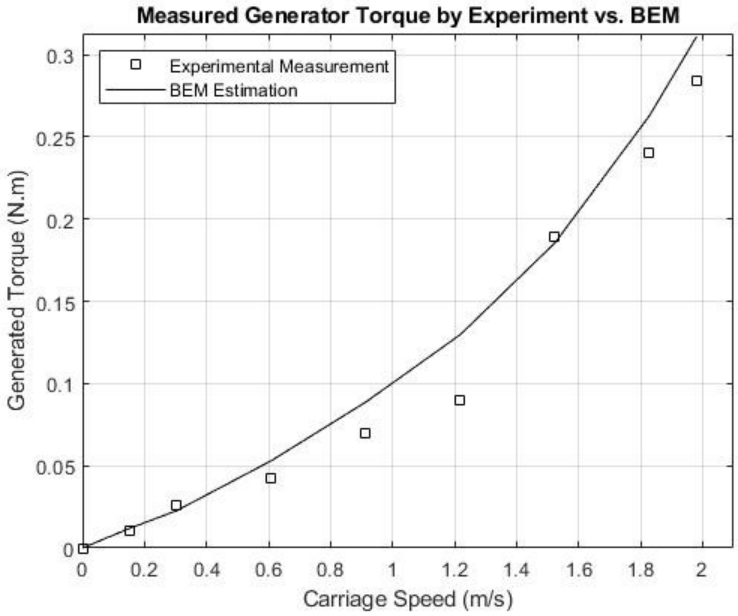


Figure 10. Comparison of torque values with increasing carriage speed from 0 to 2 m/s from experimental and BEM simulation results.

This trend aligns with our theoretical expectations, as the quantity of energy available in the moving fluid, which rises with current speed, is directly proportional to the created torque. The experimental data show that the torque was slightly less than what the BEM calculations had projected. Specifically, at 2 m/s, the BEM simulation estimated a torque of 0.3 N·m, while the experimental results indicated a torque of 0.28 N·m.

The observed discrepancy between the experimental data and the BEM simulations, though minor, suggests that the performance of the underwater current turbine may have been somewhat overstated in the BEM simulations. This discrepancy could be due to the same factors.

Despite these discrepancies, the differences between the experimental data and the BEM simulations were within a tolerable range of uncertainty, indicating that the BEM model is still a reliable tool for predicting the performance trends of the underwater current turbine.

The presented novel approach employs a comprehensive mathematical modeling method tailored specifically to propeller blade designs which facilitates the calculation of hydrokinetic loads such as torque and power. This is achieved through the segmentation of each blade and the application of a unique developed BEM algorithm. In particular, the utilization of this mathematical model allows us to make power estimations over different Re number ranges. Therefore, this helps in the optimization of the experimental OCT design by predicting nominal rotor speeds based on simulation results. Also, as shown in the Section 3, we conduct dynamometer tests. This introduced methodology for the dynamometer testing of hydrokinetic turbines represents a significant contribution that is derived from the principles of maritime engineering. The goal of this method is to standardize empirical evaluation and enhance our understanding of hydrokinetic turbine performance. Additionally, our experimental setup involves a 3D-printed turbine model enclosed in a watertight nacelle container with sensors for recording large amounts of data. The results from the analysis of the turbine's performance during the towing tank tests shows consistent correlations between the generated power, force, and rotational speed of the PMDC motor such that one can elucidate the turbine's capacity to capture dynamic energy from ocean currents.

Additionally, one can observe that the comparison between the experimental results and BEM simulations provides valuable insights. From the results, we observe discrepancies between the experimental and BEM estimations. These discrepancies are expected because the BEM algorithm cannot account for three-dimensional hydrodynamic effects due to its limitations and assumptions, such as using two-dimensional potential theory when calculating the hydrodynamic coefficients. As we utilize a two-dimensional potential flow during the development of the BEM algorithm, we are unable to capture three-dimensional effects and interactions between the fluid and structure, such as vortices' effects on the body. In essence, as can be seen in Figure 8, at lower velocities, the discrepancies are less noticeable compared to those at higher flow speeds due to three-dimensional effects. The integration of a mathematical simulation with experimental testing represents a significant contribution of this study. This research advances the field of hydrokinetic turbine technology by making a connection between mathematical models and experimental observations. We apply practical observations to harness ocean currents as a reliable and potential source of renewable energy. This interdisciplinary approach not only enhances our fundamental understanding of hydrokinetic energy conversion, but also gives a novel foundation for future advancements in the field.

One can easily observe from Figure 4 that we have an advantage in terms of the design of our scaled model of an OCT. We deliberately design and apply the shaft-propeller system relatively far away from the main body to decrease the interaction between the fluid and the main body. This helps us to reduce the interaction between the fluid effects and the main body structure. Compared to the existing literature, this gives us an advantage based on the design of our scaled model. This can open a new path focused on exploring new propeller designs and evaluating different turbine configurations to optimize efficiency and performance in future works. This could lead us to improve our design to achieve a more effective approach to conducting OCT performance analysis in future work.

In this study, we focus on improving the performance and efficiency of a small-scale underwater hydrokinetic turbine by combining detailed experimental procedures and novel mathematical modeling. During our experiments, we had some important key steps, such as precise positioning and controlled towing of the turbine model in a towing tank, real time data acquisition using various sensors, and iterative testing to refine the design. We experienced some challenges during the runs, such as towing tank length limitations and gear-head inefficiencies. We showed stable turbine performance despite these challenges. Also, when we compared our experimental results with BEM simulations, we highlighted minor discrepancies due to 3D flow effects not captured by the BEM model. In the future, we will explore different turbine design configurations, materials, and sensor technologies to further enhance hydrokinetic energy systems. Also, we could consider the environmental effects of these kinds of underwater turbines. These devices can harm marine life; for example, fish can get caught in their blades, and they can cause underwater noise. The early-stage marine renewable energy industry needs better designs and regulations. In the future, a follow-up study may be conducted to develop and test a small-scale OCT generator with a better design, aiming to minimize environmental impacts.

4. Conclusions

In conclusion, the main objective of this study is to develop and investigate the performance of a small-scale underwater OCT in terms of inflow from the perspective of optimizing hydrokinetic energy harvesting applications. This research applies a combination of mathematical modeling and experimental testing on a scaled OCT model to accurately evaluate its performance. This study ensures the turbine model's durability and reliability for underwater testing by emphasizing the construction of a watertight nacelle using 3D printing technology with a specific satisfactory material. This research aims to establish correlations between generated power, force, and rotational speed, offering valuable insights into the turbine's ability to harness dynamic energy from current through dynamometer testing in a towing tank setup. Also, we compare our experimental results

with mathematical simulations, which provides critical insights into the accuracy of our theoretical predictions in practical scenarios. This novel approach advances our understanding of hydrokinetic energy conversion and gives us a good foundation to improve our model in terms of conducting further analysis. We had a unique-novel design for understanding small-scale underwater OCT which represents a significant procedure for the performance analysis of hydrokinetic energy harvesting. We designed a unique long propeller shaft and nacelle to better evaluate the performance of the scale model. Also, this research provided a thorough evaluation of the turbine's performance by combining novel mathematical modeling with precise experimental testing. In the future, we will focus on refining our experimental methods, especially with the new nacelle design, improving our experimentation techniques, and conducting broader application studies to optimize efficiency, applicability, and repeatability. This research also supports the development of dependable renewable energy technologies to address global energy challenges while reducing environmental impacts.

Author Contributions: Conceptualization, N.I.X.; Methodology, S.R., S.S., N.I.X., E.A. and L.B.; Software, E.A.; Validation, E.A.; Formal analysis, J.I.; Investigation, S.R., S.S. and N.I.X.; Resources, N.I.X. and L.B.; Data curation, S.R. and S.S.; Writing—original draft, S.R.; Writing—review & editing, S.R., S.S., N.I.X., E.A. and J.I.; Visualization, S.S.; Supervision, N.I.X., E.A., L.B. and J.I.; Project administration, N.I.X. and L.B.; Funding acquisition, N.I.X. All authors have read and agreed to the published version of the manuscript.

Funding: The authors would like to thank the National Science Foundation (NSF) and specifically the Energy, Power, Control and Networks (EPCN) program for their valuable ongoing support in this research within the framework of grant ECCS-1809182 'Collaborative Research: Design and Control of Networked Offshore Hydrokinetic Power-Plants with Energy Storage'. The authors also wish to acknowledge the continuing support provided through the H2theFuture framework funded by the Greater New Orleans Development Foundation (08-79-05681-03)/U.S. Economic Development Administration (08-79-05681).

Institutional Review Board Statement: Not applicable.

Informed Consent Statement: Not applicable.

Data Availability Statement: The data presented in this study are available on request from the corresponding author. However, access to the data is restricted because they are part of an ongoing study. Requests for data will be reviewed and granted in accordance with the study's confidentiality and ethical guidelines.

Acknowledgments: We express our deepest thanks to George R. Morrissey and Ryan D. Thiel for their outstanding contributions and the positive impact they have had on our research endeavors. Their invaluable guidance, technical assistance, and collaborative spirit have been integral to the success of our project.

Conflicts of Interest: The authors declare no conflicts of interest.

Abbreviations

The following abbreviations are used in this manuscript:

CFD	Computational fluid dynamics
BEM	Blade Element Momentum
ICPE-CA	National Institute for Research and Development in Electrical Engineering
PIV	Particle Image Velocimetry
OCT	Ocean Current Turbine
SNMREC	Southeast National Marine Renewable Energy Center
J	Advance ratio
Fr	Froude number
U	Towing speed

Re	Reynolds number
UNO	University of New Orleans
ITTC	International Towing Tank Conference
CAD	Computer-Aided Design
PMDC	Permanent Magnet Direct Current
PETG	Polyethylene Terephthalate Glycol
PMM	Planar Motion Mechanism
RPM	Revolutions per Minute
ABS	Acrylonitrile Butadiene Styrene

References

1. Kariman, H.; Hoseinzadeh, S.; Khiadani, M.; Nazarieh, M. 3D-CFD analysing of tidal Hunter turbine to enhance the power coefficient by changing the stroke angle of blades and incorporation of winglets. *Ocean Eng.* **2023**, *287*, 115713. [CrossRef]
2. Hoseinzadeh, S.; Assareh, E.; Riaz, A.; Lee, M.; Astiaso Garcia, D. Ocean thermal energy conversion (OTEC) system driven with solar-wind energy and thermoelectric based on thermo-economic analysis using multi-objective optimization technique. *Energy Rep.* **2023**, *10*, 2982–3000. [CrossRef]
3. Ghamati, E.; Kariman, H.; Hoseinzadeh, S. Experimental and Computational Fluid Dynamic Study of Water Flow and Submerged Depth Effects on a Tidal Turbine Performance. *Water* **2023**, *15*, 2312. [CrossRef]
4. Nazarieh, M.; Kariman, H.; Hoseinzadeh, S. Numerical simulation of fluid dynamic performance of turbulent flow over Hunter turbine with variable angle of blades. *Int. J. Numer. Methods Heat Fluid Flow* **2023**, *33*, 153–173. [CrossRef]
5. Johansson, T.B.; Burnham, L. *Renewable Energy: Sources for Fuels and Electricity*; Island Press: Washington, DC, USA, 1993.
6. Dincer, I. Renewable energy and sustainable development: A crucial review. *Renew. Sustain. Energy Rev.* **2000**, *4*, 157–175. [CrossRef]
7. Owusu, P.A.; Asumadu-Sarkodie, S. A review of renewable energy sources, sustainability issues and climate change mitigation. *Cogent Eng.* **2016**, *3*, 1167990. [CrossRef]
8. Day, A.; Babarit, A.; Fontaine, A.; He, Y.P.; Kraskowski, M.; Murai, M.; Penesis, I.; Salvatore, F.; Shin, H.K. Hydrodynamic modelling of marine renewable energy devices: A state of the art review. *Ocean Eng.* **2015**, *108*, 46–69. [CrossRef]
9. Lago, L.; Ponta, F.; Chen, L. Advances and trends in hydrokinetic turbine systems. *Energy Sustain. Dev.* **2010**, *14*, 287–296. [CrossRef]
10. Khan, M.; Bhuyan, G.; Iqbal, M.; Quaicoe, J. Hydrokinetic energy conversion systems and assessment of horizontal and vertical axis turbines for river and tidal applications: A technology status review. *Appl. Energy* **2009**, *86*, 1823–1835. [CrossRef]
11. Laws, N.D.; Epps, B.P. Hydrokinetic energy conversion: Technology, research, and outlook. *Renew. Sustain. Energy Rev.* **2016**, *57*, 1245–1259. [CrossRef]
12. Kumar, D.; Sarkar, S. A review on the technology, performance, design optimization, reliability, techno-economics and environmental impacts of hydrokinetic energy conversion systems. *Renew. Sustain. Energy Rev.* **2016**, *58*, 796–813. [CrossRef]
13. Ghaffour, N.; Bundschuh, J.; Mahmoudi, H.; Goosen, M.F. Renewable energy-driven desalination technologies: A comprehensive review on challenges and potential applications of integrated systems. *Desalination* **2015**, *356*, 94–114. [CrossRef]
14. Güney, M.S.; Kaygusuz, K. Hydrokinetic energy conversion systems: A technology status review. *Renew. Sustain. Energy Rev.* **2010**, *14*, 2996–3004. [CrossRef]
15. Yuce, M.I.; Muratoglu, A. Hydrokinetic energy conversion systems: A technology status review. *Renew. Sustain. Energy Rev.* **2015**, *43*, 72–82. [CrossRef]
16. Vermaak, H.J.; Kusakana, K.; Koko, S.P. Status of micro-hydrokinetic river technology in rural applications: A review of literature. *Renew. Sustain. Energy Rev.* **2014**, *29*, 625–633. [CrossRef]
17. Ibrahim, W.; Mohamed, M.; Ismail, R.; Leung, P.; Xing, W.; Shah, A. Hydrokinetic energy harnessing technologies: A review. *Energy Rep.* **2021**, *7*, 2021–2042. [CrossRef]
18. Niebuhr, C.M.; Van Dijk, M.; Neary, V.S.; Bhagwan, J.N. A review of hydrokinetic turbines and enhancement techniques for canal installations: Technology, applicability and potential. *Renew. Sustain. Energy Rev.* **2019**, *113*, 109240. [CrossRef]
19. hee Jo, C.; young Yim, J.; hee Lee, K.; ho Rho, Y. Performance of horizontal axis tidal current turbine by blade configuration. *Renew. Energy* **2012**, *42*, 195–206. [CrossRef]
20. Ng, K.W.; Lam, W.H.; Ng, K.C. 2002–2012: 10 years of research progress in horizontal-axis marine current turbines. *Energies* **2013**, *6*, 1497–1526. [CrossRef]
21. Saini, G.; Saini, R.P. A review on technology, configurations, and performance of cross-flow hydrokinetic turbines. *Int. J. Energy Res.* **2019**, *43*, 6639–6679. [CrossRef]
22. Sarma, N.K.; Biswas, A.; Misra, R.D. Experimental and computational evaluation of Savonius hydrokinetic turbine for low velocity condition with comparison to Savonius wind turbine at the same input power. *Energy Convers. Manag.* **2014**, *83*, 88–98. [CrossRef]
23. Moshfeghi, M.; Shams, S.; Hur, N. Aerodynamic performance enhancement analysis of horizontal axis wind turbines using a passive flow control method via split blade. *J. Wind Eng. Ind. Aerodyn.* **2017**, *167*, 148–159. [CrossRef]

24. Sood, M.; Singal, S.K. Development of hydrokinetic energy technology: A review. *Int. J. Energy Res.* **2019**, *43*, 5552–5571. [CrossRef]
25. Grabbe, M. Hydro-Kinetic Energy Conversion: Resource and Technology. Ph.D. Thesis, Acta Universitatis Upsaliensis, Uppsala, Sweden, 2013.
26. Zhang, J.; Liu, S.; Guo, Y.; Guan, D.; Sun, K. Numerical Study of Performance of Horizontal-Axis Tidal Turbine with Different Configurations. In Proceedings of the 2021 9th International Conference on Smart Grid and Clean Energy Technologies (ICSGCE), Sarawak, Malaysia, 15–17 October 2021; pp. 123–130.
27. Gebreslassie, M.G.; Tabor, G.R.; Belmont, M.R. Numerical simulation of a new type of cross flow tidal turbine using OpenFOAM–Part I: Calibration of energy extraction. *Renew. Energy* **2013**, *50*, 994–1004. [CrossRef]
28. Gebreslassie, M.G.; Tabor, G.R.; Belmont, M.R. Numerical simulation of a new type of cross flow tidal turbine using OpenFOAM–Part II: Investigation of turbine-to-turbine interaction. *Renew. Energy* **2013**, *50*, 1005–1013. [CrossRef]
29. Stringer, R.M. Numerical Investigation of Cross-Flow Tidal Turbine Hydrodynamics. Ph.D. Thesis, University of Bath, Bath, UK, 2018.
30. Coiro, D.; Nicolosi, F.; De Marco, A.; Melone, S.; Montella, F. Dynamic behavior of novel vertical axis tidal current turbine: Numerical and experimental investigations. In Proceedings of the ISOPE International Ocean and Polar Engineering Conference, Seoul, Republic of Korea, 19–24 June 2005; p. ISOPE-I-05-073.
31. Coiro, D.; Maisto, U.; Scherillo, F.; Melone, S.; Grasso, F. Horizontal axis tidal current turbine: Numerical and experimental investigations. In Proceedings of the Offshore Wind and Other Marine Renewable Energies in Mediterranean and European Seas, European Seminar, Rome, Italy, 20–22 April 2006.
32. Liu, C.; Hu, C. Numerical prediction of the hydrodynamic performance of a horizontal tidal turbines. In Proceedings of the International Conference on Offshore Mechanics and Arctic Engineering, St. John's, NL, Canada, 31 May–5 June 2015; Volume 56598, p. V011T12A026.
33. Nuernberg, M.; Tao, L. Three dimensional tidal turbine array simulations using OpenFOAM with dynamic mesh. *Ocean Eng.* **2018**, *147*, 629–646. [CrossRef]
34. Chu, Y.J. A new biomimicry marine current turbine: Study of hydrodynamic performance and wake using software OpenFOAM. *J. Hydrodyn.* **2016**, *28*, 125–141. [CrossRef]
35. Stallard, T.; Collings, R.; Feng, T.; Whelan, J. Interactions between tidal turbine wakes: Experimental study of a group of three-bladed rotors. *Philos. Trans. R. Soc. A Math. Phys. Eng. Sci.* **2013**, *371*, 20120159. [CrossRef] [PubMed]
36. Alamian, R.; Shafaghat, R.; Amiri, H.A.; Shadloo, M.S. Experimental assessment of a 100 W prototype horizontal axis tidal turbine by towing tank tests. *Renew. Energy* **2020**, *155*, 172–180. [CrossRef]
37. Bahaj, A.; Batten, W.; McCann, G. Experimental verifications of numerical predictions for the hydrodynamic performance of horizontal axis marine current turbines. *Renew. Energy* **2007**, *32*, 2479–2490. [CrossRef]
38. Rourke, F.O.; Boyle, F.; Reynolds, A. Marine current energy devices: Current status and possible future applications in Ireland. *Renew. Sustain. Energy Rev.* **2010**, *14*, 1026–1036. [CrossRef]
39. Batten, W.; Bahaj, A.; Molland, A.; Chaplin, J. The prediction of the hydrodynamic performance of marine current turbines. *Renew. Energy* **2008**, *33*, 1085–1096. [CrossRef]
40. Bahaj, A.; Molland, A.; Chaplin, J.; Batten, W. Power and thrust measurements of marine current turbines under various hydrodynamic flow conditions in a cavitation tunnel and a towing tank. *Renew. Energy* **2007**, *32*, 407–426. [CrossRef]
41. Tian, W.; Ni, X.; Mao, Z.; Zhang, T. Influence of surface waves on the hydrodynamic performance of a horizontal axis ocean current turbine. *Renew. Energy* **2020**, *158*, 37–48. [CrossRef]
42. Nachtane, M.; Tarfaoui, M.; Saifaoui, D.; Rouway, M. Hydrodynamic performance evaluation of a new hydrofoil design for marine current turbines. *Mater. Today Proc.* **2020**, *30*, 889–898. [CrossRef]
43. Lust, E.E.; Bailin, B.H.; Flack, K.A. Performance characteristics of a cross-flow hydrokinetic turbine in current only and current and wave conditions. *Ocean Eng.* **2021**, *219*, 108362. [CrossRef]
44. Luznik, L.; Flack, K.A.; Lust, E.E.; Baxter, D.P. Hydrodynamic performance of a horizontal axis tidal turbine under steady flow conditions. In Proceedings of the 2012 Oceans, Hampton Roads, VA, USA, 14–19 October 2012; pp. 1–4.
45. Noruzi, R.; Vahidzadeh, M.; Riasi, A. Design, analysis and predicting hydrokinetic performance of a horizontal marine current axial turbine by consideration of turbine installation depth. *Ocean Eng.* **2015**, *108*, 789–798. [CrossRef]
46. Maganga, F.; Germain, G.; King, J.; Pinon, G.; Rivoalen, E. Experimental characterisation of flow effects on marine current turbine behaviour and on its wake properties. *IET Renew. Power Gener.* **2010**, *4*, 498–509. [CrossRef]
47. Gotelli, C.; Musa, M.; Guala, M.; Escauriaza, C. Experimental and numerical investigation of wake interactions of marine hydrokinetic turbines. *Energies* **2019**, *12*, 3188. [CrossRef]
48. LaBonte, A.; O'Connor, P.; Fitzpatrick, C.; Hallett, K.; Li, Y. Standardized cost and performance reporting for marine and hydrokinetic technologies. In Proceedings of the 1st Marine Energy Technology Symposium (METS13), Washington, DC, USA, 10–11 April 2013; pp. 10–11.
49. Nedelcu, A.; Florentina, B.; Paul Alexandru, D.; Chihaia, R.; Babutanu, C.; Marin, D.; Ciocan, G. Experimental research on a hydrokinetic turbine model. *IOP Conf. Ser. Earth Environ. Sci.* **2021**, *664*, 012061. [CrossRef]

50. Rouhi, S.; Xiros, N.; Aktosun, E.; VanZwieten, J.; Sultan, C.; Ioup, J.; Sadeqi, S. Performance Characteristics of PMDC Motor of Small-Scale Experimental Ocean Current Turbine. In Proceedings of the ASME International Mechanical Engineering Congress and Exposition, Columbus, OH, USA, 30 October–3 November 2022; Volume 5: Dynamics, Vibration, and Control; p. V005T07A066. [CrossRef]
51. Sadeqi, S.; Xiros, N.; Aktosun, E.; VanZwieten, J.; Sultan, C.; Ioup, J.; Rouhi, S. Power Estimation of an Experimental Ocean Current Turbine Based on the Conformal Mapping and Blade Element Momentum Theory. In Proceedings of the ASME International Mechanical Engineering Congress and Exposition, Virtual, 1–5 November 2021; Volume 7B: Dynamics, Vibration, and Control; p.V07BT07A004. [CrossRef]
52. Rouhi, S.; Xiros, N.; Aktosun, E.; Sultan, C.; VanZwieten, J.; Ioup, J.; Sadeqi, S. A Small-Scale Experimental Ocean Current Turbine Apparatus for Power Measurement. In Proceedings of the ASME International Mechanical Engineering Congress and Exposition, Virtual, 1–5 November 2021; Volume 7B: Dynamics, Vibration, and Control; p. V07BT07A005. [CrossRef]
53. Rouhi, S.; Sadeqi, S.; Xiros, N.; Birk, L.; Aktosun, E.; Ioup, J. Applying Artificial Intelligence to Optimize Small-Scale Ocean Current Turbine Performance. In Proceedings of the ASME International Mechanical Engineering Congress and Exposition, Columbus, OH, USA, 30 October–3 November 2022; Volume 5: Dynamics, Vibration, and Control; p. V005T07A067. [CrossRef]
54. Sadeqi, S.; Rouhi, S.; Xiros, N.; Aktosun, E.; VanZwieten, J.; Sultan, C.; Ioup, J. Numerical Investigation of an Experimental Ocean Current Turbine Based on Blade Element Momentum Theory (BEM). In Proceedings of the International Conference on Offshore Mechanics and Arctic Engineering, Virtual, 21–30 June 2021; Volume 9: Ocean Renewable Energy; p. V009T09A002. [CrossRef]
55. Rouhi, S. Towing Tank Trials of Hydrokinetic Turbine Scale Model to Support Marine Energy System Verification. Ph.D. Thesis, University of New Orleans Theses and Dissertations, New Orleans, LA, USA, 2024.
56. Sadeqi, S. Blade Design and Validation of Hydrokinetic Turbine to Harvest Water Current Energy. Ph.D. Thesis, University of New Orleans Theses and Dissertations, New Orleans, LA, USA, 2024.
57. Van Zwieten, J.; Young, M.; von Ellenrieder, K.D. Design and analysis of an ocean current turbine performance assessment system. In Proceedings of the 2012 Oceans, Hampton Roads, VA, USA, 14–19 October 2012; pp. 1–8.
58. Duerr, A.E.; Dhanak, M.R.; Van Zwieten, J.H. Utilizing the hybrid coordinate ocean model for the assessment of Florida Current's hydrokinetic renewable energy resource. *Mar. Technol. Soc. J.* **2012**, *46*, 24–33. [CrossRef]
59. VanZwieten, J.; Driscoll, F.; Leonessa, A.; Deane, G. Design of a prototype ocean current turbine—Part I: Mathematical modeling and dynamics simulation. *Ocean Eng.* **2006**, *33*, 1485–1521. [CrossRef]
60. VanZwieten, J.; Driscoll, F.; Leonessa, A.; Deane, G. Design of a prototype ocean current turbine—Part II: Flight control system. *Ocean Eng.* **2006**, *33*, 1522–1551. [CrossRef]
61. VanZwieten, J.H., Jr.; Oster, C.M.; Duerr, A.E. Design and analysis of a rotor Blade optimized for extracting energy from the Florida Current. In Proceedings of the International Conference on Offshore Mechanics and Arctic Engineering, Rotterdam, The Netherlands, 19–24 June 2011; Volume 44373, pp. 335–341.
62. Jin, Y.; Kuznetsov, A.V. Multiscale modeling and simulation of turbulent flows in porous media. *Int. J. Fluid Eng.* **2024**, *1*, 010601. [CrossRef]
63. Ijas Muhammed, V.V.; Shamsia Banu, N.; Suryan, A.; Lijo, V.; Simurda, D.; Kim, H.D. Computational study of flow separation in truncated ideal contour nozzles under high-altitude conditions. *Int. J. Fluid Eng.* **2024**, *1*, 013101. [CrossRef]

Disclaimer/Publisher's Note: The statements, opinions and data contained in all publications are solely those of the individual author(s) and contributor(s) and not of MDPI and/or the editor(s). MDPI and/or the editor(s) disclaim responsibility for any injury to people or property resulting from any ideas, methods, instructions or products referred to in the content.